

Neutron crystal-field spectroscopy and magnetic properties of $\text{DyBa}_2\text{Cu}_3\text{O}_{7-\delta}$

Peter Allenspach and Albert Furrer

*Laboratorium für Neutronenstreuung, Eidgenössische Technische Hochschule Zürich,
CH-5303 Würenlingen, Switzerland*

Fritz Hulliger

*Laboratorium für Festkörperphysik, Eidgenössische Technische Hochschule Zürich,
CH-8093 Zürich, Switzerland*

(Received 7 September 1988)

Inelastic neutron scattering has been employed to study the crystalline electric-field (CEF) interaction in the high- T_c superconductor $\text{DyBa}_2\text{Cu}_3\text{O}_{7-\delta}$. The CEF at the Dy site splits the 16-fold degeneracy of the ground-state J multiplet into eight doublet states. From the observed energy spectra we have been able to assign the four lowest excited CEF states which provided sufficient information to derive the leading CEF parameters. The results are used to predict both the direction and the size of the ordered magnetic moment in zero field, the high-field magnetization, and the Schottky anomaly of the heat capacity of $\text{DyBa}_2\text{Cu}_3\text{O}_7$, which yields reasonable agreement with the experimental data. The character of the CEF level scheme supports the application of the two-dimensional Ising model to describe the magnetic ordering of the Dy moments. From the temperature dependence of the quasielastic linewidth we conclude that the conduction electron density is negligibly small at the Dy site below T_c .

I. INTRODUCTION

It is now well known that in the high- T_c superconductor $\text{YBa}_2\text{Cu}_3\text{O}_7$ the Y ion can be replaced by most of the rare-earth ions without any appreciable effects on the superconductivity.¹⁻³ For nearly all $\text{RBA}_2\text{Cu}_3\text{O}_7$ (R denotes rare earth) compounds superconductivity and magnetic ordering coexist at low temperatures. Neutron diffraction gave evidence for three-dimensional antiferromagnetic ordering in $\text{GdBa}_2\text{Cu}_3\text{O}_7$,⁴ $\text{DyBa}_2\text{Cu}_3\text{O}_7$,^{5,6} and $\text{ErBa}_2\text{Cu}_3\text{O}_7$.⁷ In order to understand the interplay of magnetism and superconductivity in these systems, information on the magnetic ground state of the R^{3+} ions is highly desirable. Crystalline electric field (CEF) effects may play the key role in determining the magnetic ground state, since the magnetic two-ion interactions are rather small, typically of the order of T_N which is less than 1 K for most $\text{RBA}_2\text{Cu}_3\text{O}_7$ compounds. Attempts to unravel the complicated CEF level structure in these systems from the magnetic bulk properties are likely to fail, and clearly spectroscopic methods are needed to determine the CEF interaction in the low-symmetry $\text{RBA}_2\text{Cu}_3\text{O}_7$ compounds.

Very detailed information about the CEF interaction results from inelastic neutron scattering (INS) experiments. We have applied this technique to study the CEF in $\text{DyBa}_2\text{Cu}_3\text{O}_{7-\delta}$. From the observed energy spectra we have been able to identify the energies and intensities of all the ground- and excited-state CEF splittings below 20 meV, which provided sufficient information to derive the leading CEF parameters. After completion of the present work another INS study⁸ of the CEF in $\text{DyBa}_2\text{Cu}_3\text{O}_7$ appeared which, however, differs from our interpretation in various aspects, see Sec. IV. We have also determined the temperature dependence of the quasielastic linewidth

which was found to be constant below T_c and linearly increasing with temperature above T_c . Our results are discussed and used to calculate various thermodynamic magnetic properties of $\text{DyBa}_2\text{Cu}_3\text{O}_7$ and to compare them with the available experimental data.^{5,6,9-12} We conclude that the magnetic ordering of the Dy^{3+} moments is most likely of the two-dimensional Ising type as suggested by Dirken and de Jongh.¹³ A preliminary account of the present work was given in Ref. 14.

II. EXPERIMENT

The $\text{DyBa}_2\text{Cu}_3\text{O}_{7-\delta}$ sample was the same as that used in Ref. 6. It was prepared by starting from Dy_2O_3 (99.9% pure, Johnson-Matthey), BaCO_3 , and CuO (both 99% or more pure, Merck). These powders were intimately mixed by grinding them together in an agate mortar and then cold-pressed to pellets of 9-mm diameter and 1-2 mm thickness. The pellets were placed into an alumina boat which itself was introduced into a quartz tube inside a resistance furnace. The furnace was slowly heated to 1140 K while oxygen was flowing over the pellets. (All subsequent heating was carried out in oxygen atmosphere.) After 12 h at the final temperature the heating power was switched off and the material was furnace cooled. The reaction product, which was black with a slight greenish tinge, was reground and pressed and then heated again in a similar way. Contact areas between the sample Al_2O_3 boat were minimized. The oxide was now held at 1273 K for 2 h, then cooled to 570 K within 22 h including 2 h at 670 K. The resulting black and hard pellets already had a low electrical resistivity at room temperature and showed the Meissner effect above liquid-

nitrogen temperature. Nevertheless, they were reground again, pressed, and reheated to 1243 K, cooled at a rate of 20 K/h to 1073 K, faster down to 713 K, and then, within 7 h, to 573 K. The correct structure of the resulting oxide was verified with Guinier patterns taken with copper $K\alpha_1$. The onset temperature of superconductivity was determined by magnetic-susceptibility measurements to be 91 K. The final pellets had a diameter of 9–10 mm and 2–3 mm thickness. Neutron-diffraction experiments⁶ proved the single-phase character of the sample and gave an oxygen deficiency $\delta = 0.05 \pm 0.06$.

The INS experiments were performed at the reactor Saphir in Würenlingen on the triple-axis spectrometer R2. The energy of the scattered neutrons was kept fixed either at 4.8 or at 15 meV, giving rise to energy resolutions ($\Delta E = 0$) of 0.15 or 0.9 meV, respectively. To gain intensity, the measurements were carried out with use of a doubly bent graphite monochromator as well as a horizontally bent graphite analyzer, both with (002) scattering planes. Consequently, no collimations were used from neutron source to detector. Beryllium or pyrolytic graphite filters were inserted into the outgoing neutron beam to reduce higher-order contamination. The experiments were performed for moduli of the scattering vector Q and temperatures in the ranges $1 \text{ \AA} \leq Q \leq 6 \text{ \AA}^{-1}$ and $8 \text{ K} \leq T \leq 295 \text{ K}$, respectively. The $\text{DyBa}_2\text{Cu}_3\text{O}_{7-\delta}$ pellets were enclosed under He atmosphere into an Al container of dimensions $55 \times 25 \times 3 \text{ mm}^3$ which was positioned in the neutron beam in the transmission configuration.

III. RESULTS

Typical energy spectra are shown in Fig. 1. At 10 K there are two well-defined inelastic lines below 10 meV; in addition, we observe a broad and slightly structured energy distribution in the range $10 < \Delta < 30 \text{ meV}$. In the interpretation of the data we have to keep in mind that both

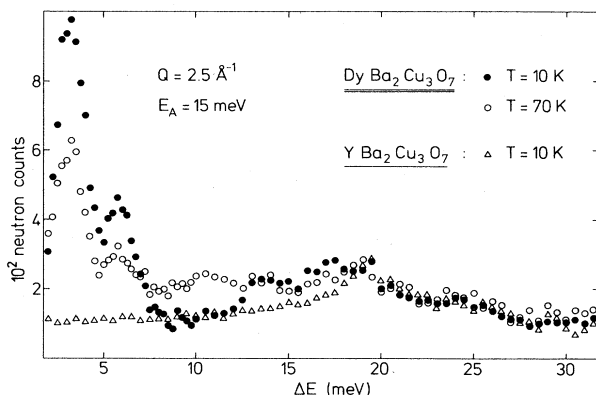


FIG. 1. Energy spectra of neutrons scattered from $\text{DyBa}_2\text{Cu}_3\text{O}_7$ and $\text{YBa}_2\text{Cu}_3\text{O}_7$. The $\text{YBa}_2\text{Cu}_3\text{O}_7$ data have been normalized to the $\text{DyBa}_2\text{Cu}_3\text{O}_7$ data by scaling to the incoherent elastic line and taking account of the different transmission factors. The 70-K data of $\text{YBa}_2\text{Cu}_3\text{O}_7$ are marginally enhanced below 10 meV compared to the 10-K data and not shown in the figure.

phonon and CEF excitations contribute to the scattering. We have measured the phonon scattering contributions for the “nonmagnetic” isostructural compound $\text{YBa}_2\text{Cu}_3\text{O}_7$ which exhibits a maximum at 19 meV (see Fig. 1); above this energy the spectral distribution observed for $\text{YBa}_2\text{Cu}_3\text{O}_7$ and $\text{DyBa}_2\text{Cu}_3\text{O}_7$ are almost identical. We can readily derive the CEF excitations by subtracting the $\text{YBa}_2\text{Cu}_3\text{O}_7$ data from the energy spectra of $\text{DyBa}_2\text{Cu}_3\text{O}_7$ as shown in Fig. 2. The 10-K data are thus characterized by four inelastic peaks at 3.3, 5.9, 14, and 17 meV which can immediately be assigned to ground-state CEF transitions. Our interpretation is confirmed by a detailed study of the peak intensities versus temperature and modulus of the scattering vector Q ; in particular, at higher temperatures the intensities of the ground-state transitions decrease, and excited CEF transitions show up as expected (see Figs. 1 and 2).

Our search for further CEF splittings turned out to be unsuccessful. We have extended our measurements up to $\Delta E = 90 \text{ meV}$ and temperatures up to 150 K, but nowhere in the observed energy spectra did we find clear-cut evidence for CEF transitions above 20 meV. This is due to the very small ground-state transition-matrix elements for the three highest CEF levels (see Table I), and their observation out of excited states failed because of the large neutron absorption of dysprosium. In fact, the intensities of the CEF transitions observed in the present work were typically an order of magnitude smaller than in similar experiments on $\text{HoBa}_2\text{Cu}_3\text{O}_7$.¹⁵

We have fitted the difference spectra by Gaussian peaks (see Fig. 2). The resulting energies of the excited CEF levels are listed in Table I. The linewidths observed at 10 K are throughout slightly broader than the instrumental

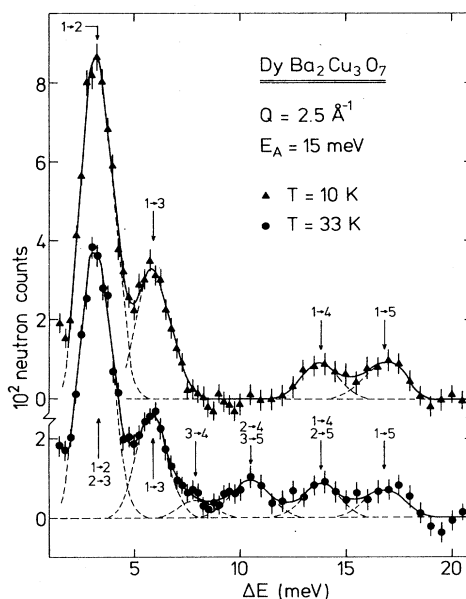


FIG. 2. Energy spectra of neutrons scattered from $\text{DyBa}_2\text{Cu}_3\text{O}_7$. The background and phonon contributions are removed by subtracting the normalized scattering from the “nonmagnetic” reference compound $\text{YBa}_2\text{Cu}_3\text{O}_7$. The curves are described in the text.

TABLE I. Ground-state transition-matrix elements and energies of the CEF states of Dy^{3+} in $\text{DyBa}_2\text{Cu}_3\text{O}_7$ calculated from the CEF parameters of Eq. (3). The energies of the observed CEF states are also listed.

$\Gamma_5^{(i)}$	$ \langle \Gamma_5^{(i)} J_\perp \Gamma_5^{(1)} \rangle ^2$	E_{calc} (meV)	E_{obs} (meV)
$\Gamma_5^{(1)}$	38.22	0	0
$\Gamma_5^{(2)}$	25.88	3.4	3.3 ± 0.1
$\Gamma_5^{(3)}$	14.75	5.9	5.9 ± 0.2
$\Gamma_5^{(4)}$	3.24	13.8	14.0 ± 0.5
$\Gamma_5^{(5)}$	2.64	16.0	17 ± 1
$\Gamma_5^{(6)}$	0.01	36.5	...
$\Gamma_5^{(7)}$	0.20	52.2	...
$\Gamma_5^{(8)}$	0.04	53.7	...

resolution, and we estimate the intrinsic linewidths of the CEF transitions to be about 0.5 meV. Upon raising the temperature the ground-state CEF transitions are contaminated by excited CEF transitions, so that a detailed analysis of the linewidth versus temperature becomes unreliable. We have therefore performed a high-resolution study of the quasielastic line up to room temperature. Typical results are shown in Fig. 3. The quasielastic data were least-squares fitted to both a Lorentzian describing the magnetic scattering from the CEF states and a Gaussian describing the incoherent elastic scattering. The Lorentzian was folded with the instrumental resolution function which was separately determined in a vanadium experiment. The temperature dependence of the intrinsic linewidth Γ of the Lorentzian is shown in Fig. 4. The

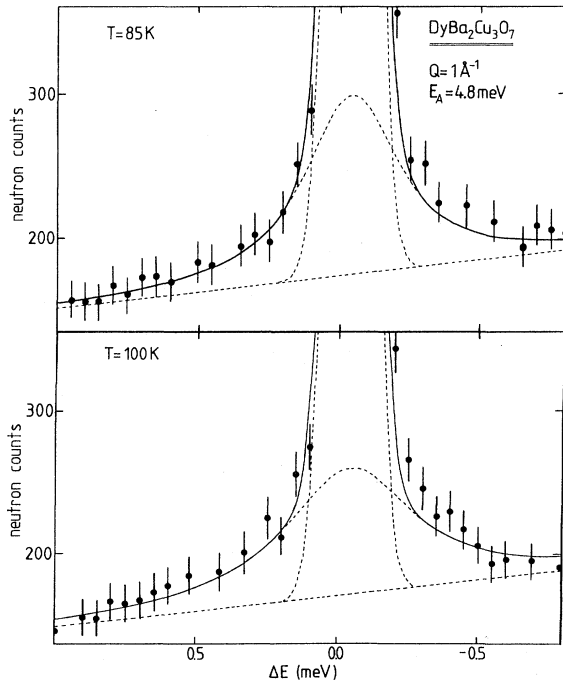


FIG. 3. Quasielastic neutron scattering from $\text{DyBa}_2\text{Cu}_3\text{O}_7$. The curves are described in the text.

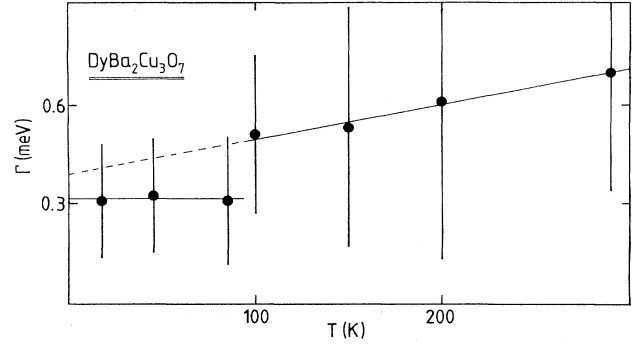


FIG. 4. Temperature dependence of the quasielastic linewidth (full width at half maximum) of $\text{DyBa}_2\text{Cu}_3\text{O}_7$. The curves are described in the text.

linewidth Γ (full width at half maximum) is essentially constant in the superconducting state and slightly increases with increasing temperature in the normal state.

IV. ANALYSIS OF RESULTS

The degeneracy of the J multiplets of a magnetic ion embedded in a crystal lattice is partly removed by the CEF potential produced by the charge distribution of the surrounding ions. The corresponding Hamiltonian for the orthorhombic symmetry D_{2h} of Dy^{3+} in $\text{DyBa}_2\text{Cu}_3\text{O}_7$ is given by

$$\mathcal{H}_{\text{CEF}} = \sum_{n=1}^3 \sum_{m=0}^n B_{2n}^{2m} O_{2n}^{2m}, \quad (1)$$

where the B_{2n}^{2m} denote the CEF parameters and the O_{2n}^{2m} are operator equivalents built up by spin operators.¹⁶ The CEF Hamiltonian (1) gives rise to a decomposition of the ground-state multiplet ${}^6\text{H}_{15/2}$ of Dy^{3+} in $\text{DyBa}_2\text{Cu}_3\text{O}_7$ into eight Kramers doublets $\Gamma_5^{(i)}$. Thus, it is impossible to derive the nine independent CEF parameters of Eq. (1) from the energies of the CEF states alone. In a first step, we, therefore, use a model with only three independent CEF parameters B_2^0 , B_4^0 , B_6^0 , whereas the remaining CEF parameters are determined by the nearest-neighbor oxygen polyhedron. In a recent study of the CEF interaction in $\text{HoBa}_2\text{Cu}_3\text{O}_7$ this model turned out to be an excellent approximation.¹⁵ We introduce the following parametrization:

$$\begin{aligned} B_2^0 F_2 &= W(1 - |y|), \\ B_4^0 F_4 &= Wxy, \\ B_6^0 F_6 &= (1 - |x|)y, \end{aligned} \quad (2)$$

with $F_2=2$, $F_4=60$, $F_6=13860$, $-1 \leq x \leq 1$ and $-1 \leq y \leq 1$. W is a scale factor. Equations (2) correspond to the most general combination of second-, fourth-, and sixth-order CEF parameters. For only one parameter set x, y the energies and transition-matrix elements of the observed CEF level scheme turned out to be in agreement with the calculated values, namely for $x \approx 0.8$, $y \approx -0.4$,

and $W < 0$. In a second step we used the corresponding CEF parameters as starting values in a least-squares fitting procedure to the observed energy spectra, in which the CEF parameters $B_2^0, B_4^0, B_4^4, B_6^0, B_6^4$ were allowed to vary independently, whereas the remaining CEF parameters were again fixed at the geometrical coordination values mentioned above. Reasonable agreement was achieved for the following CEF parameters:

$$\begin{aligned} B_2^0 &= (-1.0 \pm 0.2) \times 10^{-1} \text{ meV}, \\ B_4^0 &= (1.4 \pm 0.1) \times 10^{-3} \text{ meV}, \\ B_4^4 &= (-6.7 \pm 0.5) \times 10^{-3} \text{ meV}, \\ B_6^0 &= (1.9 \pm 0.4) \times 10^{-6} \text{ meV}, \\ B_6^4 &= (5.2 \pm 0.5) \times 10^{-5} \text{ meV}, \end{aligned} \quad (3a)$$

and

$$\begin{aligned} B_2^2 &= 0.31 B_2^0, \\ B_4^2 &= -0.24 B_4^0, \\ B_6^2 &= -0.22 B_6^0, \\ B_6^6 &= 0.22 B_6^0. \end{aligned} \quad (3b)$$

The calculated CEF level scheme is shown in Fig. 5 and in Table I which illustrates the good agreement with the observations. Table I also lists the matrix elements of all the ground-state CEF transitions which typically agree with the observed intensities within 10%–20%. We abstain from listing the wave functions of the CEF states

$$|\Gamma_5^{(i)}\rangle = \sum_{M=-J}^J a_i(M) |\pm M\rangle, \quad (4)$$

but merely mention that the ground-state wave function $|\Gamma_5^{(i)}\rangle$ is completely dominated by the $M = \pm \frac{1}{2}$ component with $a_1(\pm \frac{1}{2}) = 0.98$, i.e., the CEF interaction is expected to reduce the magnetic moment of the CEF ground-state below its free ion value by typically 30%.

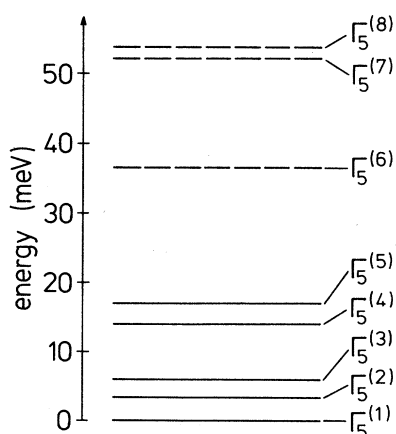


FIG. 5. Energy-level scheme of Dy^{3+} in $\text{DyBa}_2\text{Cu}_3\text{O}_7$. The solid and dashed lines correspond to the CEF levels observed in the present work and calculated from the CEF parameters of Eq. (3), respectively.

A detailed analysis of the temperature dependence of the quasielastic linewidth is severely hampered by the statistical quality of the experimental data due to the large neutron absorption of Dy (see Fig. 4). Nevertheless, we tried to analyze the observed linewidths according to the expectations outlined by Walter *et al.*¹⁷ For $T > T_c$ Korringa's law¹⁸ predicts a linear temperature dependence. The condensation of conduction electrons into Cooper pairs below T_c suppresses the electronic relaxation, as long as the crystal-field splittings of Dy^{3+} in $\text{DyBa}_2\text{Cu}_3\text{O}_7$ are smaller than the superconducting energy gap and, thus, cannot cause pair breaking of the Cooper pairs. Any residual temperature-independent linewidth may then be interpreted in terms of local distortions of the charge distribution caused by the oxygen-vacancy concentration δ . We have adopted this picture and least-squares fitted the data of Fig. 4 to a constant for $T < T_c$ and to a straight line for $T > T_c$. The results indicate a jump of the linewidths of the quasielastic CEF transitions at T_c as originally reported for Tb^{3+} ions dissolved in LaAl_2 ,¹⁹ however, more detailed experiments with improved statistics are required to unambiguously establish this particular feature.

V. MAGNETIC PROPERTIES

The CEF parameters [Eq. (3)] may not be used to calculate the magnetic properties of $\text{DyBa}_2\text{Cu}_3\text{O}_7$. The magnetic single-ion susceptibility turns out to be extremely anisotropic, yielding the c axis as the easy axis of magnetization. Indeed, neutron-diffraction studies of $\text{DyBa}_2\text{Cu}_3\text{O}_7$ gave evidence for three-dimensional antiferromagnetic ordering below 1.0 K (Ref. 5) and 0.9 K (Ref. 6) with the moments aligned along the c axis. The ordered moments were found to be considerably reduced below the free ion moment, namely $(6.8 \pm 0.1)\mu_B$ at 0.17 K (Ref. 6) and $(7.2 \pm 0.6)\mu_B$ at 0.5 K (Ref. 5) which are in good agreement with the values calculated in the mean-field approximation of $7.06\mu_B$ and $6.76\mu_B$, respectively.

References 5 and 6 also provided some zero-field magnetization data which are summarized in Fig. 6. A mean-field calculation based on the CEF parameters [Eq. (3)] clearly fails to reproduce the experimental data. On the other hand, the observed zero-field magnetization is in good agreement with Onsager's formula for the two-dimensional $S = \frac{1}{2}$ Ising model,²⁰

$$\frac{M(T)}{M(0)} = \left[1 - \sinh^{-2} \left(\frac{2J_a}{k_B T} \right) \sinh^{-2} \left(\frac{2J_b}{k_B T} \right) \right]^{0.125}, \quad (5)$$

where J_a and J_b are the magnetic nearest-neighbor interactions along the a and b axis, respectively. This model has recently been invoked¹³ to interpret the peak observed at 0.9 K in the magnetic specific heat of $\text{DyBa}_2\text{Cu}_3\text{O}_7$.^{10,21} The results of the present work give strong support for the application of this model. First, the CEF splittings between the ground state and the excited states of Dy^{3+} in $\text{DyBa}_2\text{Cu}_3\text{O}_7$ are very much larger than the magnetic ordering temperature, so that the ground-state doublet $\Gamma_5^{(1)}$ can indeed be treated in terms of an effective spin $S = \frac{1}{2}$ formalism. Second, the CEF parameters [Eq. (3)] give rise to a very anisotropic g factor of the ground state,

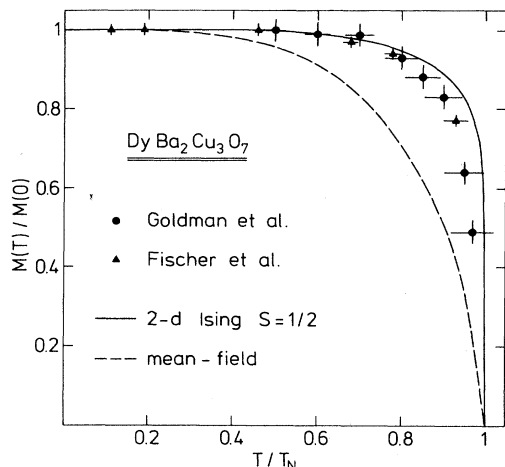


FIG. 6. Observed and calculated zero-field magnetization of $\text{DyBa}_2\text{Cu}_3\text{O}_7$.

namely $g_x=0.9$, $g_y=0.6$, $g_z=7.1$, i.e., $g_z \gg g_x, g_y$, so that the magnetic interactions between the Dy^{3+} ions can be well described by an Ising Hamiltonian. Third, the two-dimensional character of the ordering is evident when considering the large separation between neighboring Dy layers and the absence of an appreciable magnetic coupling between them.²² It follows from Eq. (5) that near T_N the magnetization obeys a power law

$$\frac{M(T)}{M(0)} = B \left(\frac{T_N - T}{T_N} \right)^\beta \quad (6)$$

with $B=1.22$ and $\beta=0.125$.²³ An analysis of the magnetization data displayed in Fig. 6 in terms of this power law yields $B=1.15$ with $\beta=0.125$ fixed. These values considerably differ from the three-dimensional $S=\frac{1}{2}$ Ising results $B \approx 1.52$ and $\beta=0.312$.²³ Guttmann, Domb, and Fox²⁴ found identical β values for $S=\frac{1}{2}$ and $S=1$, but the value of B decreases slightly for increasing S ; thus, the value of B resulting from our analysis appears to be reasonable, since the actual spin of the ground-state doublet $\Gamma_5^{(1)}$ carrying a magnetic moment of about $7\mu_B$ is certainly larger than $\frac{1}{2}$.

Next, we compare our calculations with high-field magnetization data of a powder sample⁹ measured at 4.2 K as shown in Fig. 7. The magnetization turns out to be very anisotropic as expected, so that we have to apply an averaging procedure to reproduce the observed powder magnetization data. In this procedure, we calculate the magnetization for various field directions by varying the direction cosines in a systematic manner, and then we take the average to obtain the value of the powder magnetization. The result very much depends on the number of steps n used to vary the direction cosines, and the procedure does not converge rapidly as shown in Fig. 7. For $n=2$ which corresponds to the average $\langle M \rangle = (M_x + M_y + M_z)/3$ the calculated values are below the observed magnetization data, whereas for $n > 2$ the calculated magnetization throughout exceeds the experimental data, with a difference of about $1\mu_B$ for high fields in the limit

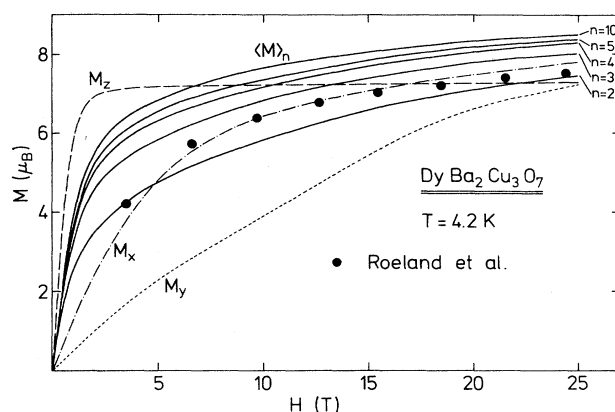


FIG. 7. Observed and calculated high-field magnetization of $\text{DyBa}_2\text{Cu}_3\text{O}_7$.

$n \rightarrow \infty$. This difference is most likely due to incomplete field penetration, since preferred orientation effects have to be ruled out due to the immobilization of the powder sample with stycast in the magnetization experiments.⁹ It is interesting to notice that the average $\langle M \rangle_{n \rightarrow \infty}$ exceeds M_z for $H \geq 6$ T, which means that the z axis is the easy axis of magnetization only for low fields. Our calculations indeed indicate that for $H \geq 2.5$ T the easy axis of magnetization gradually moves from the z axis towards the x axis in the xz plane, and it would be interesting to verify this prediction in a single-crystal experiment.

Finally, we use the CEF parameters [Eq. (3)] to calculate the Schottky anomaly of the specific heat which exhibits a shallow maximum at 20 K with $\Delta C=5.8$ J/mol K. This is in qualitative agreement with observed heat-capacity data reported by van der Meulen *et al.*¹¹ and Dunlap *et al.*¹² who found $\Delta C_{\text{max}}=4.5$ J/mol K at 20 K and $\Delta C_{\text{max}}=3.7$ J/mol K at 16 K, respectively. We do not expect to obtain perfect quantitative agreement between the calculated and observed heat-capacity data, since the latter are the result of a correction procedure which takes account of the electronic and phonon contributions.

VI. CONCLUSIONS

We have been able to establish the CEF level scheme of Dy^{3+} in $\text{DyBa}_2\text{Cu}_3\text{O}_7$ below 20 meV with use of the INS technique and to rationalize our results in terms of model parameters. Our CEF parameters [Eq. (3)] are in reasonable agreement with the values derived from INS experiments by Culverhouse *et al.*⁸ except for the sixth-order terms which roughly differ by a factor of 2. While this difference has little effect on the energies of the low-lying CEF levels, it considerably changes the overall CEF splitting as well as the wave functions of the CEF states, except for the ground-state doublet $\Gamma_5^{(1)}$. Thus, the low-temperature magnetic properties discussed in Sec. V cannot be used to discriminate between the two CEF parameter sets, but the parameters of Ref. 8 produce CEF transition-matrix elements which are incompatible with our neutron spectroscopic observations.

Calculations of some magnetic properties of $\text{DyBa}_2\text{Cu}_3\text{O}_7$ on the basis of our CEF parameters are in reasonable agreement with the experimental data and strongly support the two-dimensional Ising character of the magnetic interaction suggested in Ref. 13. What is needed now are measurements of the magnetic properties on single-crystalline samples to further check the proposed CEF parameters. In particular, a detailed study of the H - T phase diagram would be highly desirable to examine the field-induced change of the easy direction of magnetization predicted in Sec. V.

According to Korringa's law¹⁸ the slope $\Delta\Gamma/\Delta T$ of the quasielastic linewidth is related to the conduction electron density $N(E_F)$. The fact that we observe a zero slope for $\text{DyBa}_2\text{Cu}_3\text{O}_7$ below T_c indicates a zero or negligibly small value of $N(E_F)$. A similar behavior of the linewidth was observed for $\text{ErBa}_2\text{Cu}_3\text{O}_7$ (Ref. 17) and $\text{NdBa}_2\text{Cu}_3\text{O}_7$ (Refs. 25 and 26), and from low-temperature ¹⁵⁵Gd Mössbauer measurements on $\text{GdBa}_2\text{Cu}_3\text{O}_7$ (Ref. 27) an extremely low value of $N(E_F)$ was derived. In view of these results the magnetic interactions in the $\text{RBa}_2\text{Cu}_3\text{O}_7$ compounds (where R is a rare-earth element) are clearly not of the Ruderman-Kittel-Kasuya-Yosida type, but superexchange and dipolar interactions should be appropriate to describe the magnetic ordering.²⁷

Let us finally discuss the question whether there is some systematic behavior of the CEF parameters in the whole $\text{RBa}_2\text{Cu}_3\text{O}_7$ series. To do so we write the CEF parameters in the following way:

$$B_{2n}^{2m} = a_{2n}^{2m} \langle r^{2n} \rangle \chi_{2n} \gamma_{2n}^{2m}, \quad (7)$$

where $\langle r^{2n} \rangle$ denotes the $2n$ th moment of the radial distribution of the $4f$ electrons, χ_{2n} is a reduced matrix element, γ_{2n}^{2m} a geometrical coordination factor,²⁸ and a_{2n}^{2m} a reduced CEF parameter. We may anticipate constant values of a_{2n}^{2m} through the whole rare-earth series, since the CEF is expected to be determined mainly by the coordination polyhedra which are known to be unaffected by the rare-earth ions in these systems.¹² This is the idea of the superposition model introduced by Newman,²⁹ which has recently been discussed by Nekvasil³⁰ for the

TABLE II. Reduced CEF parameters a_{2n}^0 (in units of 10^4 meV Å) of $\text{RBa}_2\text{Cu}_3\text{O}_7$ compounds determined by INS experiments.

$\text{RBa}_2\text{Cu}_3\text{O}_7$	Ref.	a_2^0	a_4^0	a_6^0
$\text{DyBa}_2\text{Cu}_3\text{O}_7$	This work	0.7	3.0	4.1
	Ref. 24	0.5	4.0	9.2
$\text{HoBa}_2\text{Cu}_3\text{O}_7$	Ref. 10	0.9	3.8	8.8
	Ref. 24	0.2	3.2	8.8
	Ref. 33	0.6	3.9	8.8
$\text{ErBa}_2\text{Cu}_3\text{O}_7$	Ref. 24	0.5	4.9	11.5
	Ref. 34	0.2	4.8	12.0

$\text{RBa}_2\text{Cu}_3\text{O}_7$ compounds. Table II lists the reduced CEF parameters a_{2n}^0 for all those $\text{RBa}_2\text{Cu}_3\text{O}_7$ compounds which have been studied by neutron spectroscopy and subsequently analyzed on the basis of the CEF Hamiltonian (1). The geometrical coordination factors γ_{2n}^0 were calculated for the nearest-neighboring oxygen shell,¹⁵ and for the radial integrals $\langle r^{2n} \rangle$ we used the values tabulated by Lewis.³¹ The simple point-charge model predicts $a_2^0 = a_4^0 = a_6^0$, which is clearly not realized. Surprisingly, there is also a large spread of the a_{2n}^0 values for a particular degree $2n$, and only the reduced CEF parameter a_4^0 appears to be roughly constant for the $\text{RBa}_2\text{Cu}_3\text{O}_7$ compounds considered in Table II. This means that the application of the superposition model to extrapolate the CEF interaction to other $\text{RBa}_2\text{Cu}_3\text{O}_7$ compounds should be considered with caution, which is supported by the analysis of recent INS experiments on $\text{NdBa}_2\text{Cu}_3\text{O}_7$.^{25,26,32}

ACKNOWLEDGMENTS

We are indebted to Dr. P. Fischer for useful discussions. Financial support by the Swiss National Science Foundation is gratefully acknowledged.

- ¹P. H. Hor, R. L. Meng, Y. Q. Wang, L. Gao, Z. J. Huang, J. Bechtold, K. Forster, and C. W. Chu, Phys. Rev. Lett. **58**, 1891 (1987).
²M. B. Maple, K. N. Yang, M. S. Torikachvili, J. M. Ferreira, J. J. Neumeier, H. Zhon, Y. Delichaouch, and B. W. Lee, Solid State Commun. **63**, 635 (1987).
³F. Hulliger and H. R. Ott, Z. Phys. B **68**, 291 (1987).
⁴D. McK. Paul, H. A. Mook, A. W. Hewart, B. C. Sales, L. A. Boatner, J. R. Thompson, and M. Mostoller, Phys. Rev. B **37**, 2341 (1988).
⁵A. I. Goldman, B. X. Yang, J. Tranquada, J. E. Crow, and C. S. Jee, Phys. Rev. B **36**, 7234 (1987).
⁶P. Fischer, K. Kakurai, M. Steiner, K. N. Clausen, B. Lebech, F. Hulliger, H. R. Ott, P. Brüesch, and P. Unternährer, Physica C **152**, 145 (1988).
⁷T. Chattopadhyay, P. J. Brown, D. Bonnenberg, S. Ewert, and H. Maletta, Europhys. Lett. **6**, 363 (1988).
⁸S. R. Culverhouse, B. D. Rainford, D. McK. Paul, L. Caves, R.

- Osborn, and B. Frick, J. Magn. Magn. Mater. (to be published).
⁹L. W. Roeland, F. R. de Boer, Y. K. Huang, A. A. Menovskii, and K. Kadowaki, Physica C **152**, 72 (1988).
¹⁰B. W. Lee, J. M. Ferreira, Y. Dalichaouch, M. S. Torikachvili, K. N. Yang, and M. B. Maple, Phys. Rev. B **37**, 2368 (1988).
¹¹H. P. van der Meulen, J. J. M. Franse, Z. Tarnawski, K. Kadowaki, J. C. P. Klaasse, and A. A. Menovsky, Physica C **152**, 65 (1988).
¹²B. D. Dunlap, M. Slaski, D. G. Hinks, L. Soderholm, M. Beno, K. Zhang, C. Segre, G. W. Crabtree, W. K. Kwok, S. K. Malik, I. K. Schuller, J. D. Jorgensen, and Z. Sungaila, J. Magn. Magn. Mater. **68**, L139 (1987).
¹³M. W. Dirken and L. J. de Jongh, Solid State Commun. **64**, 1201 (1987).
¹⁴A. Furrer, P. Allenspach, and F. Hulliger, J. Magn. Magn. Mater. **76 & 77**, 594 (1988).
¹⁵A. Furrer, P. Brüesch, and P. Unternährer, Physica C **153-**

- 155, 164 (1988); Solid State Commun. **67**, 69 (1988); Phys. Rev. B **38**, 4616 (1988).
- ¹⁶K. W. H. Stevens, Proc. Phys. Soc. London, Sect. A **65**, 209 (1952).
- ¹⁷U. Walter, S. Fahy, A. Zettl, S. G. Louie, M. L. Cohen, P. Tejedor, and A. M. Stacy, Phys. Rev. B **36**, 8899 (1987).
- ¹⁸J. Korrying, Physica **16**, 601 (1950).
- ¹⁹R. Feile, J. K. Kjems, M. Loewenhaupt, and H. E. Hoenig, Phys. Rev. Lett. **47**, 610 (1981).
- ²⁰L. Onsager, Phys. Rev. **65**, 117 (1944).
- ²¹A. P. Ramirez, L. F. Schneemeyer, and J. V. Waszczak, Phys. Rev. B **36**, 7145 (1987).
- ²²J. van den Berg, C. J. van der Beek, P. H. Kes, J. A. Mydosh, G. J. Nieuwenhuys, and L. J. de Jongh, Solid State Commun. **64**, 699 (1987).
- ²³M. E. Fisher, Rep. Prog. Phys. **30**, 671 (1967).
- ²⁴A. J. Guttmann, C. Domb, and P. F. Fox, J. Phys. (Paris), Colloq. **32**, C1-354 (1970).
- ²⁵U. Walter, E. Holland-Moritz, A. Severing, A. Erle, H. Schmidt, and E. Zirngiebl, Physica C **153-155**, 170 (1988).
- ²⁶P. Allenspach, A. Furrer, P. Brüesch, and P. Unternährer, Physica B **156 & 157**, 864 (1988).
- ²⁷H. H. A. Smit, M. W. Dirken, R. C. Thiel, and L. J. de Jongh, Solid State Commun. **64**, 695 (1987).
- ²⁸M. T. Hutchings, in *Solid State Physics*, edited by F. Seitz and D. Turnbull (Academic, New York, 1964), Vol. 16, p. 227.
- ²⁹D. J. Newman, Adv. Phys. **20**, 197 (1971).
- ³⁰V. Nekvasil, Solid State Commun. **65**, 1103 (1988).
- ³¹W. B. Lewis, in *Magnetic Resonance and Related Phenomena*, edited by I. Ursu (Publishing House of Academy of Romania, Bucharest, 1971), p. 717.
- ³²E. Gering, B. Renker, F. Gompf, D. Ewert, H. Schmidt, R. Ahrens, M. Bonnet, and A. Dianoux, Physica C **153-155**, 184 (1988).
- ³³A. Goldman, Y. Gao, S. T. Ting, J. E. Crow, W. H. Li, and J. W. Lynn, J. Magn. Magn. Mater. **76 & 77**, 607 (1988).
- ³⁴P. Allenspach, predoctoral thesis, Eidgenössische Technische Hochschule Zürich, 1988 (unpublished).